Biomass Pellet Breakage: A Comparison Between Contact Models

Hamid Gilvari[1], Wiebren de Jong[2], Dingena L. Schott[1]

[1]Section of Transport Engineering & Logistics, Department of Maritime & Transport Technology, Faculty of Mechanical, Maritime & Materials Engineering, Delft University of Technology

[2]Section of Large Scale Energy Storage, Department of Process & Energy, Faculty of Mechanical, Maritime and Materials Engineering, Delft University of Technology
Mekelweg 2, 2628 CD, Delft, the Netherlands

h.gilvari@tudelft.nl

Keywords Biomass Pellets, Breakage Behaviour, Contact Models, DEM, Compression

Abstract

The breakage behaviour of biomass pellets with a diameter of 6 mm under uniaxial compression testing conditions was studied experimentally and numerically using the discrete element method (DEM). Two types of the available bonding contact models in EDEM software were used to compare the macroscopic properties including the maximum stress at failure, strain at failure, and the pellet Young's Modulus. The models were based on 1) the Timoshenko beam theory and 2) a bonded particle model. The results showed that both models reasonably predict the maximum stress values, however, the bonded contact model was not able to predict the strain at failure and the Young's Modulus measured experimentally.

1 INTRODUCTION

The worldwide trade of biomass pellets is rapidly increasing while the transportation system is lagging behind. Biomass pellets, due to their fragile nature, may fracture during transportation and storage and generate fine particles. Generation of fine particles causes material loss, equipment fouling, increase the risk of fire, and increase the environmental pressures. Different biomass pellets show different breakage behavior regarding their physical properties. High strength pellets could tolerate higher forces resulting in a less brittle nature. However, the physical properties of biomass pellets have been less studied by the researchers and the breakage behavior is not fully understood yet.

The individual material strength can be measured using different compression methods, e.g. the uniaxial compression test. In a typical compression test, the force-displacement data is derived from the compression device and based on the data the stress-strain curves are obtained. The curve is useful for further investigation on the maximum stress limit, strain at failure and calculating the Young's Modulus which is derived from the linear portion of the curve.

The breakage behavior, and more specifically the stress-strain curves of biomass pellets during compression can be investigated experimentally or numerically. The Discrete Element Method (DEM) has successfully been applied as a powerful numerical method for studying different characteristics of various materials. In DEM, the specimen which is the object of the study, is created by using multi-particle configurations where the particles interact with each other following their contact models. Each contact model in DEM has its own specifications and parameters, therefore, the results may vary depending on the contact model specifications. A calibrated model of an individual biomass pellet could be used for

further numerical investigation on the bulk material behaviour during transportation and handling.

There are many contact models created by different researchers embedded in different tools to simulate the breakage behaviour. The EDEM software created by EDEM Solutions® is a commercial one which has defined a bonding contact model based on the work of Potyondy and Cundall [1]. The model is defined only for bonded particles, therefore, it is needed to couple it with another contact model for the non-bonded particles (either non-bonded at all or broken bonds). In the software, different built-in contact models could be coupled with the bonded particle model, of which the Hertz-Mindlin model is one of the most popular. The software also supports using the application programming interface (API) which enables the user to introduce external contact models. Recently, researchers at the University of Edinburg developed the Edinburgh Bonded Particle Model (EBPM) contact model based on the Timoshenko beam theory [2], which connects every two neighbouring particles through a beam and uses the Hertz-Mindlin model for non-bonded particles [3].

The aim of this research is to firstly characterize the macroscopic properties of a type of torrefied biomass pellet and secondly, to compare the results of two different available contact models namely the bonded contact model (BCM), and EBPM. Although DEM is proven as a powerful tool to study the breakage behaviour of different materials and many researchers have used it in their researches, to the best of the authors' knowledge, the breakage behaviour of biomass pellets has been never investigated numerically and this is the first paper to use DEM for that purpose.

2 MATERIALS AND METHODS

2.1 Material

The biomass pellet used in this study was a torrefied mixed-wood pellet produced in the UK. Further information about the torrefaction and densification processes was not disclosed. The measured properties of the pellets are shown in Table 1. The lengths and diameters were determined based on CEN/TS 335 [4] and the moisture content according to CEN/TS 14961 [5]. The pellet density was calculated based on the pellet mass and volume, which were measured using a laboratory scale and a caliper, respectively.

Table 1: Properties of the material used in this study

Material	**Diameter (mm)**	**Length (mm)**	**Moisture Content (%)**	**Pellet density (kg/m^3)**
Torrefied Mixed Wood pellet	6	Between 10 to 30	9.7	1304

2.2 Methods

2.2.1 Experimental

The individual pellet strength under uniaxial compression test conditions was measured by means of an Instron 5500R compression device. Each pellet was polished at both ends using sandpaper in order to vertically stand on the Instron plate. This also ensures that the compressive force applies evenly to both surfaces of the pellets. The force-displacement data was recorded for each sample. The stress (σ_a) and the strain (ε_a) at each time-step were calculated using the equations (1) and (2), respectively.

$$\sigma_a = \frac{F}{\pi r^2} \quad (1)$$

$$\varepsilon_a = \frac{l_0 - l}{l_0} \quad (2)$$

where F is the force, r is the pellet radius, l_0 is the initial pellet length, and l is the displacement length. The Young's Modulus was calculated using the linear portions of the stress-strain curves. The test was executed five times with pellets of different lengths.

2.2.2 Modelling

2.2.2.1 Theory

The EDEM software was used in this study to perform the simulations. The so-called "EBPM" and Hertz-Mindlin with bonding models were used in this study. The EBPM model considers a cylindrical beam between the centres of each two neighbouring particles and bonds them with a pre-defined bond Young's Modulus and Poisson's ratio. Each bond shares 6 degrees of freedoms at each end which allows compression, tension, and shear forces and torques as illustrated in Figure 1.

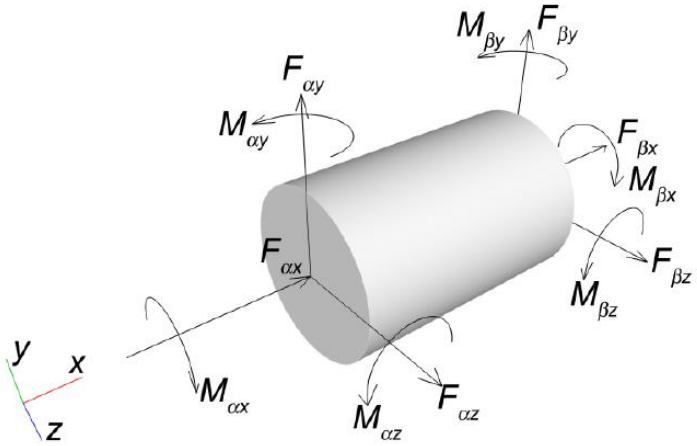

Figure 1: A typical bond in EBPM in the local co-ordinate system and the forces and momentums on the edges (adapted from [6])

The bonds will be generated between every two particles which their virtual radii overlap. The virtual radii are determined using a contact radius multiplier which multiplies the physical particle radius. Therefore, in addition to the physical radius, there is a virtual one which determines the bonding domain. Only one bond can exist between every two particles and once a bond breaks it will never generate one again. The bonds are allowed to tolerate the compression, shear, and tension forces up to a pre-defined threshold. The bonds existence will be checked at each time-step and once any of these three thresholds is reached, the bond will break and the contact between the particles will follow the Hertz-Mindlin contact model.

The calculation of the force and momentum for bonding particles is based on the Timoshenko beam theory and is calculated at each time-step according to equation (3):

$$\{\Delta F\} = [K].\{\Delta u\} \quad (3)$$

Where ΔF is the force vector and Δu is the displacement vector and [K] is the stiffness matrix as shown in equations (4) to (6):

$$\{\Delta F\} = \{\Delta F_{\alpha x}\, \Delta F_{\alpha y}\, \Delta F_{\alpha z}\, \Delta M_{\alpha x}\, \Delta M_{\alpha y}\, \Delta M_{\alpha z} \Delta F_{\beta x}\, \Delta F_{\beta y}\, \Delta F_{\beta z}\, \Delta M_{\beta x}\, \Delta M_{\beta y}\, \Delta M_{\beta z}\}^T \quad (4)$$

$$\{\Delta u\} = \{\Delta d_{\alpha x}\, \Delta d_{\alpha y}\, \Delta d_{\alpha z}\, \Delta \theta_{\alpha x}\, \Delta \theta_{\alpha y}\, \Delta \theta_{\alpha z} \Delta d_{\beta x}\, \Delta d_{\beta y}\, \Delta d_{\beta z}\, \Delta \theta_{\beta x}\, \Delta \theta_{\beta y}\, \Delta \theta_{\beta z}\}^T \quad (5)$$

$$K = \begin{bmatrix} K_1 & -K_2 & -K_1 & -K_2 \\ K_2 & K_3 & -K_2 & K_4 \\ -K_1 & K_2 & K_1 & K_2 \\ K_2 & K_4 & -K_2 & K_3 \end{bmatrix} \quad (6)$$

where

$$[K_1] = \begin{bmatrix} \frac{E_b A_b}{L_b} & 0 & 0 \\ 0 & \frac{12k}{L_b^{\,2}(1+\Phi)} & 0 \\ 0 & 0 & \frac{12k}{L_b^{\,2}(1+\Phi)} \end{bmatrix} \quad (7)$$

$$[K_2] = \begin{bmatrix} 0 & 0 & 0 \\ 0 & 0 & \frac{-6k}{L_b(1+\Phi)} \\ 0 & \frac{6k}{L_b(1+\Phi)} & 0 \end{bmatrix} \quad (8)$$

$$[K_3] = \begin{bmatrix} \frac{k}{(1+v_b)} & 0 & 0 \\ 0 & \frac{k(4+\Phi)}{(1+\Phi)} & 0 \\ 0 & 0 & \frac{k(4+\Phi)}{(1+\Phi)} \end{bmatrix} \quad (9)$$

$$[K_4] = \begin{bmatrix} \frac{-k}{(1+v_b)} & 0 & 0 \\ 0 & \frac{k(2-\Phi)}{(1+\Phi)} & 0 \\ 0 & 0 & \frac{k(2-\Phi)}{(1+\Phi)} \end{bmatrix} \quad (10)$$

where E_b, v_b, A_b, L_b, Φ, are the bond Young's Modulus, Poisson ratio, bond's cross-section area, bond length, and the Timoshenko bond coefficient, and k is calculated from the equation (11)

$$k = \frac{E_b I_b}{L_b} \quad (11)$$

where I_b is the second moment of area of the bond and is calculated from equation (12).

$$I_b = \frac{r_b^4 \pi}{4} \quad (12)$$

More details about the EBPM model implementation can be found in [3, 7].

The other contact model, which is based on Hertz-Mindlin with bonding, is characterised by bonding particles with a finite-size glue bond. The created bonds include a normal and a shear stiffness while they can resist normal and tangential movements up to critical normal and shear stresses. Once the bond meets either one or two of these thresholds, it fails and the

particles will follow the Hertz-Mindlin model. For simplicity, this model is called "BCM" in the rest of this paper. After bonding, the forces and torques on the particles are set to zero and will be calculated at every time-step according to equations (13) to (16):

$$\delta F_n = -v_n S_n A \delta t \quad (13)$$

$$\delta F_{nt} = -v_t S_t A \delta t \quad (14)$$

$$\delta M_n = -\omega_n S_t J \delta t \quad (15)$$

$$\delta M_t = -\omega_t S_n \frac{J}{2} \delta t \quad (16)$$

where

$$A = \pi R_B^2 \quad (17)$$

$$J = \frac{1}{2}\pi R_B^4 \quad (18)$$

Where R_B, S_n, S_t, δt are the bond radius, the normal and shear stiffness, and the time-step, respectively. v_n and v_t are the normal and tangential velocities and ω_n and ω_t are the normal and tangential angular velocities.

The bonds will break at any time-step for which one of the normal or tangential stresses reaches the critical stress as shown in equations (19) and (20):

$$\sigma_{max} < \frac{-F_n}{A} + \frac{2M_t}{J} R_B \quad (19)$$

$$\tau_{max} < \frac{-F_t}{A} + \frac{M_n}{J} R_B \quad (20)$$

The Hertz-Mindlin contact model is based on the equations (21):

$$F_n = \frac{4}{3} E^* \sqrt{R^*} \delta_n^{\frac{3}{2}} \quad (21)$$

Where the E^* stands for the equivalent Young's Modulus and R^* stands for the equivalent radius and are calculated by:

$$\frac{1}{E^*} = \frac{(1-\nu_i^2)}{E_i} + \frac{(1-\nu_j^2)}{E_j} \quad (22)$$

$$\frac{1}{R^*} = \frac{1}{R_i} + \frac{1}{R_j} \quad (23)$$

Where E_i, ν_i, R_i and E_j, ν_j, R_j are the Young's Modulus, the Poisson ratio, and the radius of each sphere in contact, respectively.

2.2.2.2 Model Inputs

In order to make a comparison between the two contact models mentioned, all the particle properties and simulation specifications were kept constant for all the simulations. This includes the pellet generation, the number of spheres and the spheres size distribution in a pellet assembly, the coordination of the spheres, the properties of the spheres, time-step, and compression rate. Table 2 shows all the constant properties and their values in the simulations. It should be highlighted that there is no overlap between the particles in a pellet assembly.

Table 2: Model inputs for particles and wall geometry (symbols are shown in parentheses)

Particle Properties	**Unit**	**Value**	**Wall properties (Steel)**	**Unit**	**Value**
Initial pellet length (l_0)	mm	20	Density	kg/m^3	7850
Pellet radius (r)	mm	3	Poisson ratio	-	0.3
Number of spheres	-	961	Young's Modulus (E_w)	Pa	1.976e+11
Maximum sphere radius	mm	0.44	Coefficient of restitution (C_{R,w^*})	-	0.0001
Minimum sphere radius	mm	0.33	Coefficient of static friction (μ_{s,w^*})	-	1
Density (ρ_p)	kg/m^3	2645	Rolling friction (μ_{r,w^*})	-	0
Poisson ratio(ν_p)	-	0.25	Compression rate	mm/s	50
Young's Modulus (E_p)	Pa	1.5e+10			
Coefficient of restitution (C_{R,p^*})	-	0.5	**Other Properties**	**Unit**	**Value**
Coefficient of static friction (μ_{s,p^*})	-	0.5	Contact radius multiplier	mm	1.2
Rolling friction (μ_{r,p^*})	-	0.5	Time-step (δt)	s	7.5e-08

*p: particle-particle
*w: particle-wall

The bonding properties of the models were calibrated by trial end error, so that both models could represent roughly the same stress on the real pellets. The calibrated properties are given in Table 3. The calculation of the stress and strain was similar to the experimental part, i.e. the stress value was calculated using the equation (1) where the force value is the mean of the forces on two compression plates and the strain value calculated based on the initial positions of the plates (l_0) and the displacement of the pellet (plate positions plus the total overlap between the plates and the spheres). Young's Modulus was measured using the linear portion of the stress-strain curves.

Table 3: Bonding properties of both models

EBPM	**Value**	**BCM**	**Value**
Bond Young's Modulus (Pa)	5.5e08	Bond Normal Stiffness (N/m^3)	1e10
Bond Poisson ratio	0.3	Bond Shear Stiffness (N/m^3)	8e08
Maximum Compressive Stress (Pa)	7e07	Critical Compressive Stress (Pa)	8e08
Maximum Tensile Stress (Pa)	3.5e07	Critical Shear Stress (Pa)	8e08
Maximum Shear Stress (Pa)	1.5e07		

3 RESULTS

3.1 Experimental

The results of the experimental compression testing are shown in Figure 2. As can be seen clearly, pellets show different behaviour during the compression test which results in different stress-strain curves. This is due to the heterogeneity in the structure of the pellets which is linked to the raw material characteristics and the pelletization process specifications. The pellet heterogeneity was also reported by the other researchers who measured the maximum stress at failure for different types of biomass pellets during axial

compression [8]. Table 4 shows the stress-strain and the Young's Modulus of the pellets and their standard deviations. As shown, there is no correlation between neither the pellet lengths and stress at failure nor the stress and the Young's modulus. This makes the calibration of the numerical part very complex and difficult as the numerical results should be consistent with the experimental results. Therefore, for simplifying the calibration, the mean values of the results are considered as the benchmark for the numerical investigation.

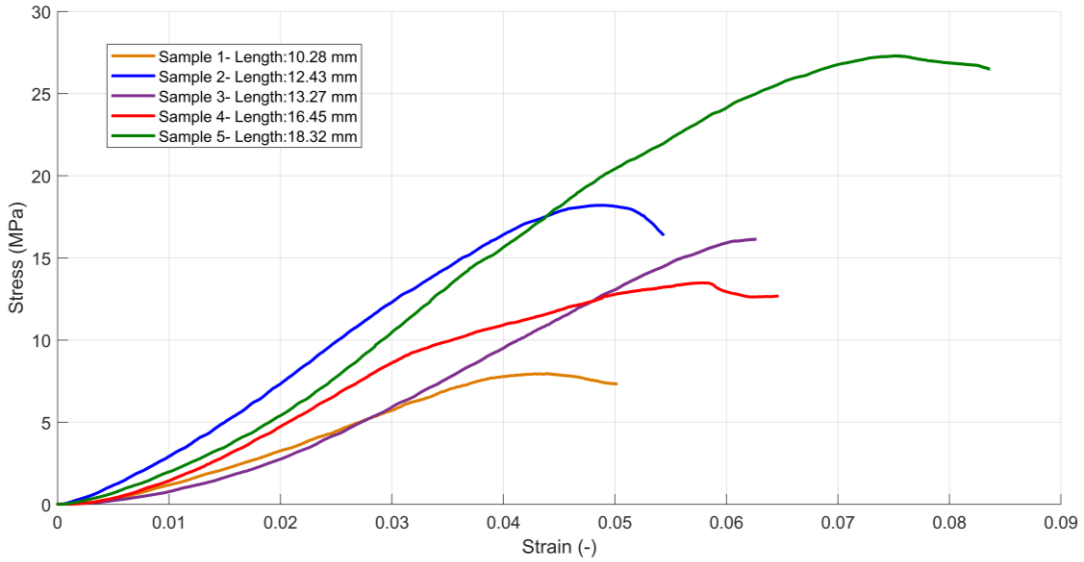

Figure 2: Experimental results of the uniaxial compression test with five different pellets

Table 4: The results of the compression tests (the standard deviations are shown in parentheses)

Sample Number	Length (mm)	Stress at Failure (MPa)	Strain at Failure	Young's Modulus (MPa)
1	10.28	7.96	0.045	190.4
2	12.43	18.20	0.049	422.7
3	13.27	16.15	0.063	229.6
4	16.45	13.49	0.058	340.7
5	18.32	27.3	0.075	437.4
μ	-	16.62 (6.3)	0.058 (0.01)	324.1 (99.6)

3.2 Numerical

Using the same assembly of the pellet and contact radius multiplier of 1.2 mm, around 4000 bonds were created in each model. This means that the mean coordination number for the spheres in the assembly is 4.16. Figure 3 shows a typical pellet under compression in EDEM. The yellow lines between the spheres show the bonds between them. The results of the stress-strain curves of both EBPM and BCM are given in Figure 4 where the values are given in Table 5.

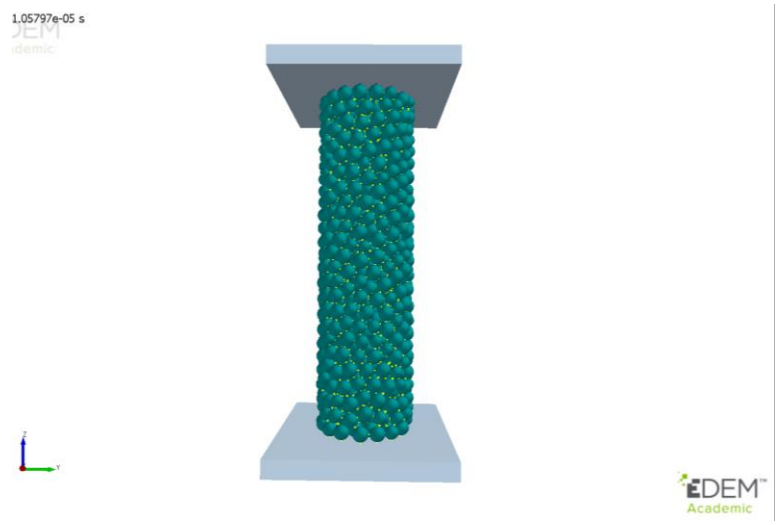

Figure 3: Assembly of a pellet using 961 spheres under compression

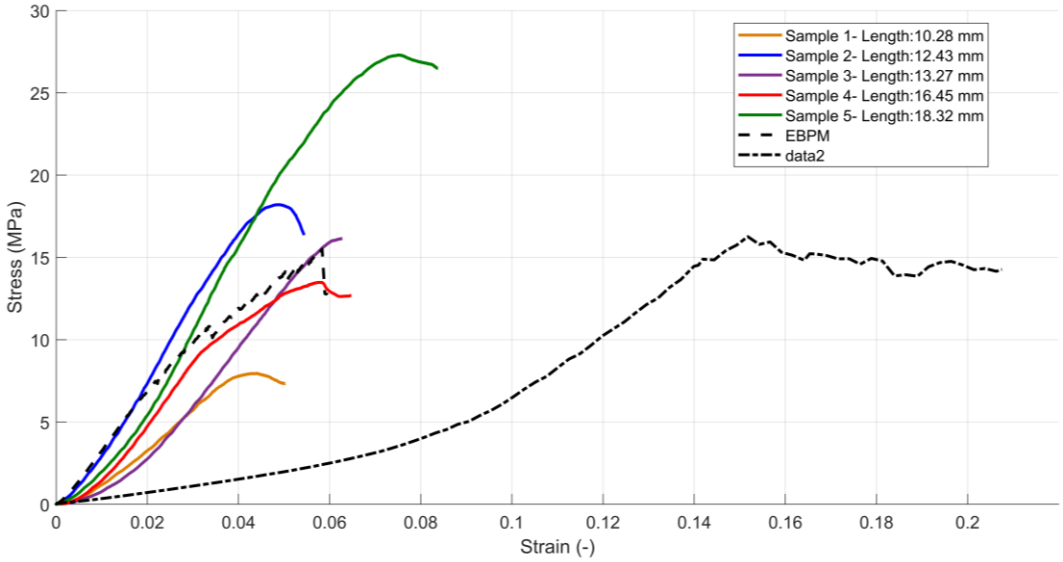

Figure 4: Stress-strain results of experimental and numerical methods

Table 5: Results of the macroscopic properties of the numerical models

Contact Model	Stress at Failure (MPa)	Strain at Failure	Young's Modulus (MPa)
EBPM	15.50	0.058	367.7
BCM	16.26	0.152	41.8

As can be clearly seen, both models reasonably predict the maximum stress at failure, however, the BCM is not capable to predict the strain at failure and consequently the Young's Modulus. This was further investigated by executing more simulations on the effect of bond normal and shear stiffness on the strain value at failure and Young's Modulus. The normal stiffness of 5e+09 and 5e+10 (N/m^3) and shear stiffness of 1e+09 and 6e+08 (N/m^3) were used in the other simulations. However, as can be seen in Figure 5, a higher or lower bond stiffness has no effect on the results unless the stress at failure. Kemeny [9], in his paper on rock deformation, claimed that the origins of the crack growth under compression are small regions of tension. This was also confirmed by the other researchers [1, 6] who

investigated the strength of the concrete cylinders. Looking at the breakage patterns of the models, in BCM, all the bonds could only fail due to compression or shear. However, in EBPM, the bonds are mostly broken due to tension. In BCM, manipulating the bonding properties will change the value of stress at failure for biomass pellets, however, the strain value is always higher than the experimental results most probably because there is no source for the crack generation inside the pellet due to tension. Figure 6 shows the number of broken bonds due to compression, shear, or tensile stresses in EBPM and total broken bonds in BCM up to the failure point.

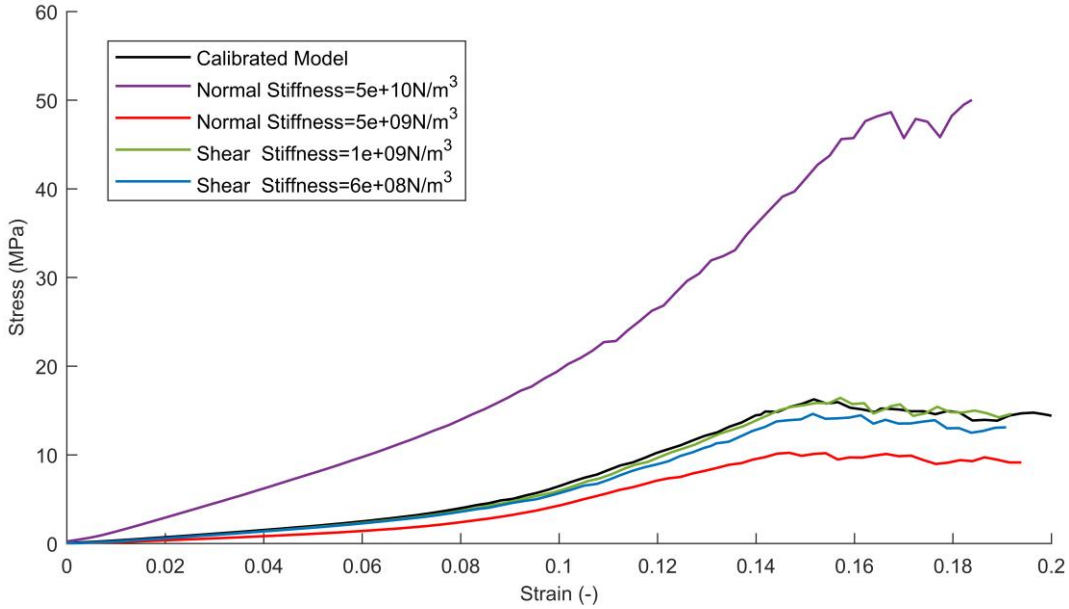

Figure 5: Effect of normal and shear stiffness of BCM on the stress-strain curve

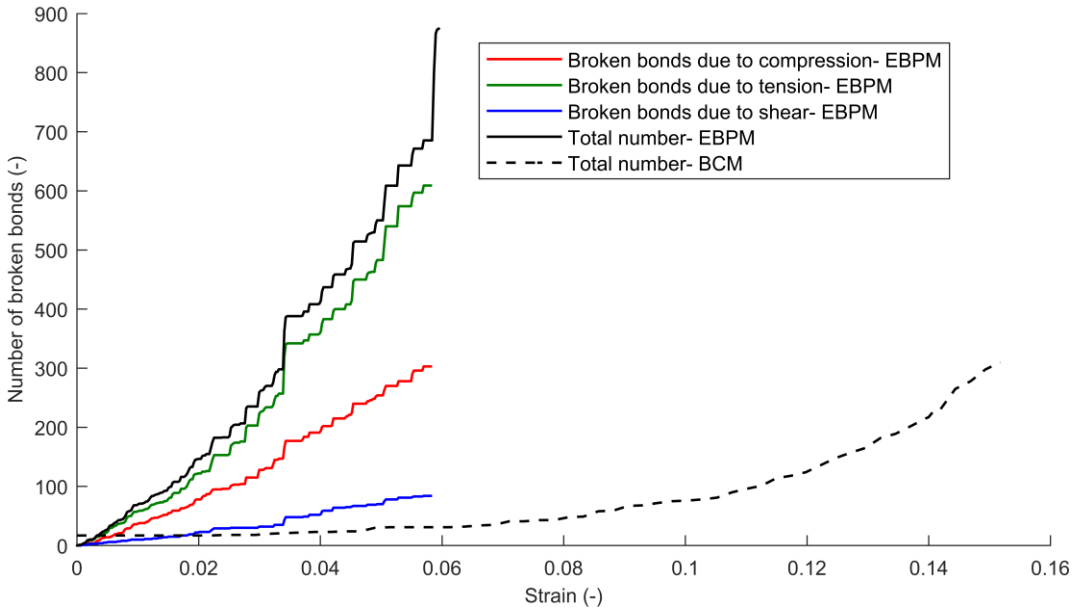

Figure 6: Number of broken bonds up to failure using BCM and EBPM models

In order to confirm the results of EBPM, more simulations with different values of tensile strengths were executed in this work. For that, a tensile strength of 1e+07 and 7e+07 Pa was used. The results are shown in Figure 7. As can be seen clearly, changing the critical tensile strength will change the strain at failure because of a change in the bond breakage patterns. Table 6 shows the number of broken bonds at failure for each simulation. As shown, the total

number of broken bonds is less than the sum of the compression, tension, and shear failure because in some cases the bonds fail due to more than one type of failure e.g. a bond may break due to compression and tension in the same time-step. Looking at the table, when using a low tensile strength (1e+07 Pa), most of the bonds break early in the simulation resulting in a low stress at failure. By increasing the tensile strength value (3.5e+07 Pa), the bonds will not break early in the simulation resulting in higher stress values while other types of failure play a role. By using a very high value of tensile strength (7e+07 Pa) the bonds will not break due to tension then the origin of crack generation is restricted. Therefore, similar to BCM, the EBPM model overestimates the strain at failure.

Table 6: Number of broken bonds at failure for each simulation with EBPM

Tensile Strength (Pa)	Broken bonds due to compression	Broken bonds due to tension	Broken bonds due to shear	Total number of broken bonds
1e+07	32	785	0	785
3.5e+07	303	609	84	658
7e+07	638	85	635	1140

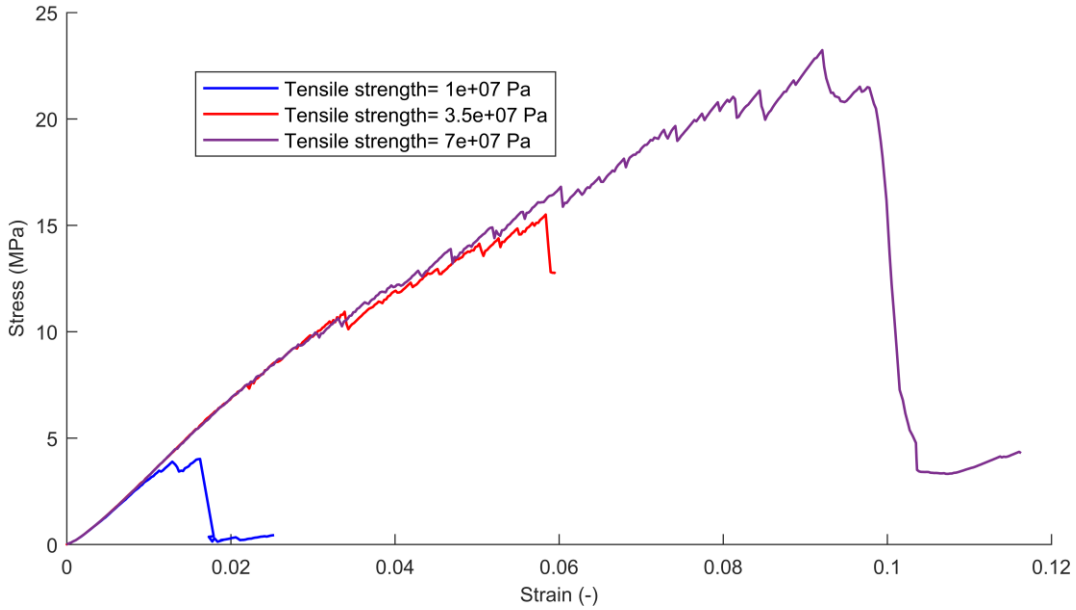

Figure 7: Effect of tensile strength on the stress-stain curve of EBPM

4 CONCLUSION

The breakage behaviour of a selected type of torrefied biomass pellet under uniaxial compression test was experimentally characterized and numerically simulated using two available bonding contact models available in EDEM software namely EBPM and BCM. One of the main differences between the contact models is the capability of EBPM to represent bond failure via tension. We showed that although both models can truly predict the stress values at failure, the BCM is not able to reasonably predict the experimental strain values and the Young's Modulus of the pellets. This is because the bonds can only fail due to compression and shear while the main bond failure mechanism in uniaxial compression test is tension. However, as in EBPM most of the bonds fail due to tension, the generation of the cracks happens before failure which results in predicting the experimentally measured strain values well. Therefore, the EBPM model is recommended for further investigation of biomass pellet breakage in operational conditions.

5 ACKNOWLEDGMENT

The authors would like to thank the laboratory technicians of Material Science and Engineering department of TU Delft, Elise Reinton and Ton Riemslag for their support with the experimental part.

REFERENCES

1. Potyondy, D.O. and P. Cundall, *A bonded-particle model for rock.* International journal of rock mechanics and mining sciences, 2004. **41**(8): p. 1329-1364.
2. Timoshenko, S.P., *X. On the transverse vibrations of bars of uniform cross-section.* The London, Edinburgh, and Dublin Philosophical Magazine and Journal of Science, 1922. **43**(253): p. 125-131.
3. Brown, N.J., *Discrete element modelling of cementitious materials*. 2013, The University of Edinburgh.
4. *CEN/TS 335 Solid biofuels-Methods for the determination of particle size distribution-part1: Oscillating screen method using sieve apertures of 3.15 mm and above*. 2005, European Committee for Standardization.
5. *CEN/TS - 14961 - Solid biofuels - Fuel specifications and classes - Part 1: General requirements*. 2005, European Committee for Standardization.
6. Brown, N.J., J.-F. Chen, and J.Y. Ooi, *A bond model for DEM simulation of cementitious materials and deformable structures.* Granular Matter, 2014. **16**(3): p. 299-311.
7. Brown, N.J., J.P. Morrissey, and J.Y. Ooi, *EDEM Contact Model: Timoshenko Beam Bond Model*, T.U.o. Edinburgh, Editor. 2015, EDEM Solutions.
8. Williams, O., S. Taylor, E. Lester, S. Kingman, D. Giddings, and C. Eastwick, *Applicability of mechanical tests for biomass pellet characterisation for bioenergy applications.* Materials, 2018. **11**(8): p. 1329.
9. Kemeny, J.M., *A model for non-linear rock deformation under compression due to sub-critical crack growth.* International journal of rock mechanics and mining sciences & geomechanics abstracts, 1991. **28**(6): p. 459-467.